Dissolution Kinetics or Pure Mass Transfer? A Mechanistic Study of Dissolution

Erik Kaunisto, Mariagrazia Marucci, and Anders Axelsson
Dept. of Chemical Engineering, LTH, Lund University, SE-221 00 Lund, Sweden

DOI 10.1002/aic.12475
Published online December 17, 2010 in Wiley Online Library (wileyonlinelibrary.com).

In many cases, classic in vitro tests are used to investigate dissolution from powders and solids. A problem with these kinds of tests is the frequent use of agitation, leading to a lumped description of the properties at the solid–liquid interface. The hydrodynamic forces arising from agitation might have a nontrivial impact on the dissolution properties, thus calling for a comparison of results with those stemming from stagnant dissolution with the aim to increase the understanding of the dissolution process. Stagnant dissolution of compressed solid benzoic acid was examined using the noninvasive electronic speckle pattern interferometry technique in this study. The diffusion coefficient for benzoic acid in 37°C water was measured using the same technique, and, by combining the results, the surface kinetics at the solid–liquid interface were calculated. A comparison with previous dissolution data from a rotating disk suggests that the presence of convection can increase the observed surface kinetics. © 2010 American Institute of Chemical Engineers *AIChE J,* 57: 2610–2617, 2011
Keywords: dissolution, ESPI, benzoic acid, mass transfer, mathematical modeling

Introduction

Solubility and dissolution rates of drug substances are important parameters to quantify in drug-delivery development work. This has become more important due to the introduction of substances of low solubility, often having hydrophobic characteristics. Furthermore, it is important to fully understand the dissolution process mechanistically. This understanding simplifies the drug formulation design and the in vitro as well as the *in vivo* release characteristics can be explained.

The explanation of experimental results obtained from standard dissolution tests[1] often relies on models[2–5] that cannot substantially quantify the different release mechanisms, resulting in lumped dissolution-rate coefficients which include not only possible dissolution kinetics but also, depending on the formulation, mass-transfer hindrance within the porous matrix and/or within the boundary layer adjacent to the solid surface. Furthermore, dissolution methods often use convective transport by means of flowing liquid or by agitation in a vessel. This is a way to reduce the external mass-transfer hindrance through the boundary layer although still present. The influence of hydrodynamics is at least two-fold:

1 The boundary layer thickness is influenced.

2 The hydrodynamic force may affect the kinetics at the solid surface or add mechanical erosion of the formulation.

The latter phenomenon could make the measured dissolution constant somewhat ambiguous. Thus, to avoid these kinds of artifacts and to fully understand the dissolution process, there is a need to find experimental techniques able to discriminate between different dissolution mechanisms. One way is to study stagnant dissolution without agitation if the dissolution concentration profile can be measured. Concentration profiles can be obtained by using, holographic interferometry (HI) or electronic speckle pattern interferometry (ESPI). HI and ESPI have also been successfully used to measure diffusion coefficients in liquids for binary systems,[6–8] in gels,[9–13] and in membranes.[14,15] Importantly, HI has been recently used to study a dissolving mineral in stagnant water.[16] However, as

Correspondence concerning this article should be addressed to A. Axelsson at anders.axelsson@rektor.lth.se.
The first two authors contributed equally to this work.

far as we know, this approach has not yet been used to characterize the dissolution of a drug. Moreover, ESPI has never been used to investigate the dissolution process of a drug.

This study relies on the use of ESPI to determine stagnant concentration profiles. To discriminate between the mechanisms of dissolution rate and external mass transfer, two types of experiments are performed in the same diffusion cell:

1 First, the diffusion mass-transfer rate is determined in the diffusion cell evaluated as diffusion coefficients from concentration profiles obtained when the substance diffuses from a dense solution to a dilute solution.

2 Second, the same type of experiment is performed but with the substance being released from a solid surface of the compressed substance inserted into the diffusion cell.

Thus, the only difference in the experimental setups is the dissolution kinetics from the solid surface as the diffusive mass transfer in the stagnant liquids should be the same. Benzoic acid was used as a model substance due to its similarity to many pharmaceutical substances.

Theory

Theory of ESPI

The theory of ESPI will be briefly summarized in this section. A more detailed description has been presented earlier.[17–19] In ESPI, an object beam and a reference beam are combined. The resulting intensity distribution, $I(x,y)$, neglecting the proportional factor, is given at each point in the image by:

$$I(x,y) = |U_1(x,y) + U_2(x,y)|^2 = U_1^2(x,y) + U_2^2(x,y) + 2 \cdot U_1(x,y) \cdot U_2(x,y) \cdot \cos\phi \quad (1)$$

where I is the intensity at any point, U_1 is the complex electrical field of the reference beam, U_2 is the complex electrical field of the object beam, ϕ is the phase difference between the object beam and the reference beam, and (x,y) is the position on the CCD chip. Any changes in the optical length of the reference beam or the object beam cause a change in the intensity distribution. By subtracting an image from another image and taking the modulus, an image with fringes reflecting the change in the phase difference is obtained. The intensity distribution is:

$$|\Delta I| = 4 \cdot U_1(x,y) \cdot U_2(x,y) \cdot \left|\sin\left(\phi + \frac{\delta}{2}\right) \cdot \sin\left(\frac{\delta}{2}\right)\right| \quad (2)$$

where δ represents the change in phase difference between the reference and the object beams. Dark fringes appear when $|\Delta I|$ is equal to zero. For a one-dimensional system, the intensity data contained in each pixel are averaged over a certain number of adjacent pixels (N) along a line for which $\frac{\delta}{2}$ is constant, which is the direction perpendicular to diffusion in this particular case. The averaged intensity can then be expressed as:

$$|\Delta I| = 4U_1(x,y) \cdot U_2(x,y) \cdot \left|\sin\left(\frac{\delta}{2}\right)\right| \cdot \frac{1}{N} \cdot \sum_N \left|\sin\left(\phi + \frac{\delta}{2}\right)\right| \quad (3)$$

As the random phase difference ϕ is uniformly distributed over all the values between 0 and 2π, $\frac{1}{N} \cdot \sum_N \left|\sin\left(\phi + \frac{\delta}{2}\right)\right|$ approaches a constant value if N is sufficiently large. Dark fringes appear when $\frac{\delta}{2} = m\pi$, where $m = 0,\pm1,\pm2,\ldots$. This means that dark fringes appear when the difference in optical path length between the object and the reference beam, equals an integer multiple of the wavelength (λ).

Calculation of refractive index and concentration above the tablet

In this work, a dissolution study was performed in a release cell as illustrated in Figure 1a. In such a cell, a solid substance is dissolved in a stagnant liquid. During the dissolution process, the concentration of the dissolved substance in the cell changes, and so does the refractive index, n, creating a subsequent change in the difference in the optical path lengths between the beams, Δa.

The interference pattern was obtained in the following way. Before the dissolution experiment was started, the cell was filled with water. When the temperature in the cell was stable, a first image, the reference image, was obtained. To avoid natural convection,[20] the tablet, made by compaction of the solid substance, was not put on top of the cell on immobilized water. Instead, the cell was emptied and the tablet was inserted at the bottom of the cell. Then the cell was filled again with water, followed by a quick water immobilization due to the narrow cell. Thus, there was no significant convection present during the dissolution process as can be seen by the obtained agreement between model and experimental data. Images were then taken at regular intervals. Interference patterns were obtained by subtracting an image obtained when dissolution had progressed for a certain period of time, from the image obtained at time zero, i.e., the reference image. A schematic interference pattern is shown in Figure 2.

The fringe furthest away from the interface is labeled No. 1; the other fringes are numbered consecutively toward the interface. At the first fringe, the optical path of the laser beam has been altered by one wavelength as compared with the light passing through the unaffected part of the liquid. The optical path difference between two consecutive fringes, Δa, also equals one wavelength. Therefore, at the ith fringe, the total optical path change can be expressed as:

$$\Delta a_i = i \cdot \lambda \quad i = 0,1,2.. \quad (4)$$

Δa_i can be described as a change in the refractive index:

$$\Delta n_i = \frac{\Delta a_i}{b} = \frac{i \cdot \lambda}{b} \quad i = 0,1,2.. \quad (5)$$

where b is the cell thickness. When a linear dependency exists between the refractive index and the concentration over the range studied, it is easy to calculate the difference in concentration between the ith fringe and the unaffected region of the cell:

$$\Delta c_i = g \cdot \Delta n_i = g \cdot \frac{i \cdot \lambda}{b} \quad i = 0,1,2.. \quad (6)$$

In Eq. 6, g equals $\frac{\Delta c}{\Delta n}$.

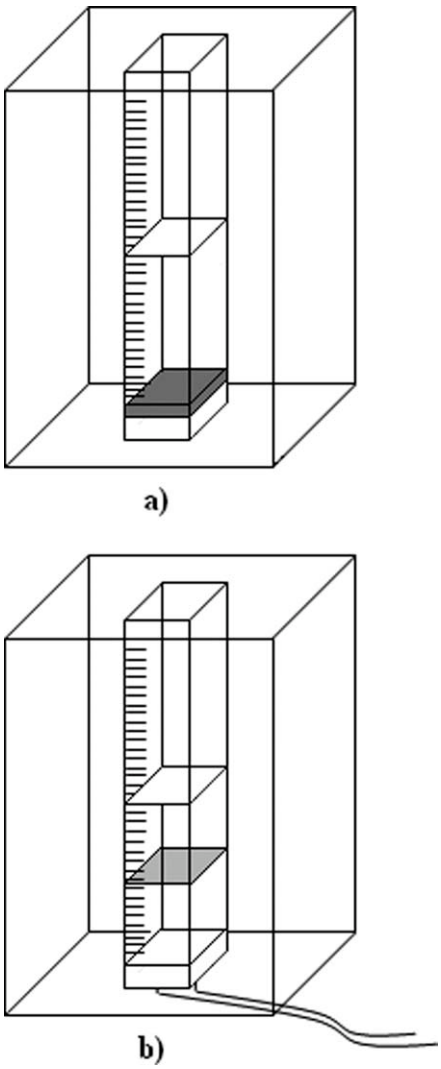

Figure 1. Schematic representation of the diffusion/dissolution cell.

(a) The dissolution cell with a tablet in the bottom of the cell (dark gray) and water above the tablet (white). (b) The diffusion cell with the low and high density solutions in the top and bottom of the cell, respectively (white). The liquid–liquid interface is also shown (light gray). The bottom pipe is used to introduce the liquid of a high concentration.

A mathematical model for tablet dissolution

A one-dimensional model was used to simulate the dissolution profile obtained in the holographic cell:

$$\frac{\partial c}{\partial t} = D\frac{\partial^2 c}{\partial X^2} \tag{7}$$

Boundary conditions:

$$-D\frac{\partial c}{\partial X}|_{X=0} = k_s(c_{\text{sat}} - c)$$

$$\frac{\partial c}{\partial X}|_{X=L} = 0$$

$$c|_{t=0} = 0$$

The dynamic diffusion Eq. 7 with boundary conditions was solved over the domain, using finite element discretization. The model was solved for benzoic acid, using a measured diffusion coefficient and solubility literature data,[21] $c_{\text{sat}} = 40.7$ mol/m^3, as model parameters.

The model Eq. 7 does not take into account the dissociation kinetics of benzoic acid nor any pH effects,[22] and it is assumed that the acid and its corresponding base can be regarded as a single diffusing species.[23] The boundary condition at the tablet interface represents the flux from dissolution, assuming a first-order reaction with respect to the total solubility and the total interfacial concentration of substance, respectively. Further, it is assumed that the process can be described by a single rate constant, k_s, representing the surface kinetics. The surface kinetics can be considered a sum of all the kinetic processes at the tablet interface, wetting, fusion, and solvation.[24]

A Neumann boundary condition is used at a distance $X = L$ from the tablet interface, where no concentration gradients are present. Because pure water was used, the initial concentration of benzoic acid was zero.

The surface kinetics was estimated in MATLAB[25] by using the nonlinear optimization toolbox coupled with Comsol Multiphysics.[26] The objective was to minimize the concentration residual sum of squares, $\text{RSS} = \sum_i \left(c_{\text{mod},i} - c_{\text{exp},i}\right)^2$, between model and experiments at the discrete fringe positions.

Materials and Methods

Materials

Pure aqueous dissolution media and crystalline benzoic acid (Merck 99.95%) were used in all of the experiments.

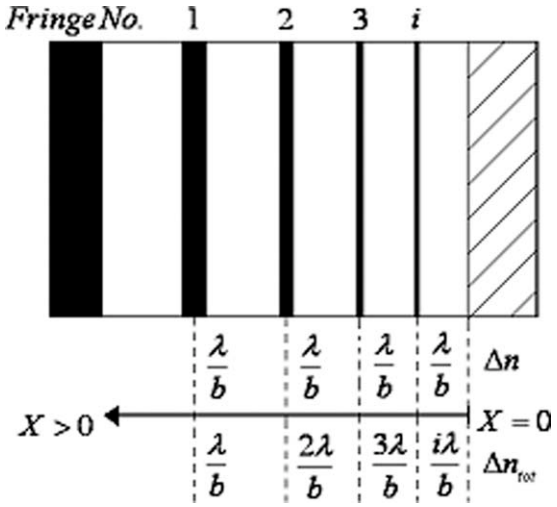

Figure 2. Schematic representation of the interference pattern.

The individual and cumulative changes in refraction index, Δn and Δn_{tot}, are shown. X denotes the perpendicular distance from the tablet surface.

Measurement of diffusion coefficient of benzoic acid in liquid

The diffusion coefficient of benzoic acid dissolved in water was measured by ESPI according to a methodology described in detail elsewhere.[15] Each experiment was started by filling half of the cell with the low-density solution, followed by pumping the more dense solution from below with a slowly moving piston giving the very low flow rate of 10 cm^3/h, as seen in Figure 1b. The low-density solution was pure water, $c_{low} = 0$, and the high-density solution, $c_{high} = 29$ mol/m^3. The concentrations were chosen to match the concentration range obtained in the diffusion cell when the dissolution experiments were performed and also to avoid precipitation in the handling of the dissolved substance. Thus, the diffusion coefficient obtained was representative of the solution present on top of the tablets in the dissolution experiments. The difference in density and the low flow rate assured that no mixing would occur in the cell, and that the fluid interface would move as a plug by a velocity of $\sim 5.6 \times 10^{-3}$ cm/s. If mixing would occur no fringes would be obtained; consequently, the results obtained could not have been affected by mixing. Even convective mixing due to a temperature gradient would cause the fringes to disappear. The cell was 6 cm high, 0.5 cm thick, and 1 cm wide. Vertical fringes were introduced in the system by rotating a glass plate located after the spatial filter. A typical pattern consisting of two distinct turns of fringes (discussed in relation to Figure 4) was obtained as the pictures taken before and after vertical fringe introduction were subtracted. The diffusion in the liquid can be calculated by Eq. 8, using the turning point distance, z, and t_{1d} and t_{2d}, representing the points in time when the images were taken[7]:

$$D = \frac{z^2}{8} \cdot \frac{\left(\frac{1}{t_{1d}} - \frac{1}{t_{2d}}\right)}{\ln\left(\frac{t_{2d}}{t_{1d}}\right)} \tag{8}$$

Experiments were run at 37°C in duplicate. The temperature was kept constant by using circulated heated water at 37°C. Temperature stability was ensured to avoid temperature oscillations that can significantly shift the obtained interference pattern. Temperature stability in the current setup has been shown in earlier work.[14]

Refractive index measurements

An automatic refractometer (RFM 81, Bellingham, England) was used to measure the relationship between concentration and refractive index for benzoic acid at 37°C. The refractometer operated at a wavelength of 589 nm, which was considered sufficiently close to the wavelength of the laser in the ESPI setup. For benzoic acid, $g = \frac{\Delta c}{\Delta n}$ was constant within the range of concentrations used in the dissolution experiment (between 0 and 40.7 mol/m^3) and was found to be 2.41×10^{-5} m^3/mol.

ESPI setup and experimental procedure

Figure 3 shows the ESPI experimental setup. A continuous-wave He-Ne laser (2.5 mW power output, 25 LHP 691, Melles Griot, USA) emitting coherent light at 632.8 nm was used as light source. The light passed through a half-wave plate (M-MT-RS, Newport Corp., USA) and was divided into a reference beam and an object beam by a polarizing beam splitter. The object beam passed through a half-wave plate rotated by 45° (M-MT-RS, Newport Corp., USA), located after the beam splitter. Thus, the reference and object beams had the same vertical polarization. Each beam passed through a three-axis spatial filter with a 10× objective and a 25μm pinhole (M-900, Newport Corp., USA). The object beam traveled through a glass plate, the diffusion cell, and an achromatic lens (f = 90 mm, 32 22 89, Spindler & Hoyer, Germany). The two beams were combined with a pellicle (03 BPL 003) and impinged on the CCD array with an angular difference of less than 1°. The images were recorded using a cooled CCD camera (CoolSNAP-Pro color camera, Media Cybernetics, USA). This 36-bit color interline camera was equipped with a Bayer color mask. The total image area contained 1324 × 1040 pixels, each with a size of 4.65 μm. The CCD camera was focused on the external surface of the diffusion cell, which was fitted with a ruler.

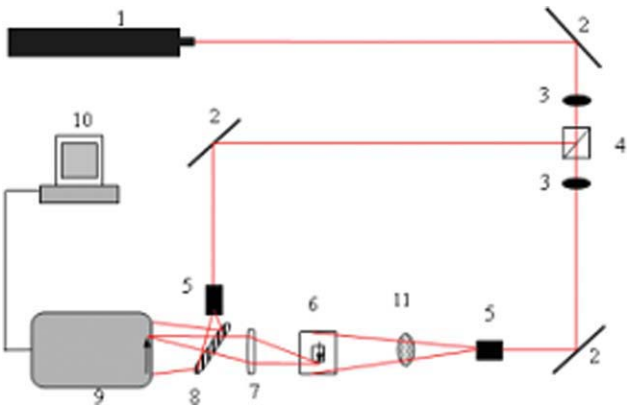

Figure 3. Experimental setup for ESPI.

(1) He-Ne laser, (2) mirror, (3) half-wave plate, (4) beam splitter, (5) spatial filter, (6) diffusion cell, (7) achromatic lens, (8) pellicle, (9) CCD camera, (10) computer for image analysis, and (11) glass plate. [Color figure can be viewed in the online issue, which is available at wileyonlinelibrary.com.]

First, the diffusion cell was filled with a solution having the same concentration as that used in the dissolution experiments. A reference image was obtained when the temperature of the diffusion cell was stable. The cell was then emptied and the tablet was placed inside the cell. The dissolution experiment started when the cell was filled with the dissolution medium. Images were obtained at ~1 and 2 h from the start of the experiments. Typically, the image acquisition time was extremely short, 0.01–0.02 s. Interference patterns were obtained by subtracting images obtained during the dissolution experiment from the reference image. The inference patterns were analyzed using the image analysis software Image Pro Plus 4.1 (Media Cybernetics).

Tablet compression

Benzoic acid crystals were ground manually. Powder (0.4 g) was compressed within a 12-mm-cylindrical tablet punch. A pressure of 1000 kg was applied for 1 min, and then slowly lowered to avoid tablet cracks. The tablets were shaped into 10 mm × 10 mm × 3 mm blocks, which were used in the dissolution experiments. The tablet surface was slightly smaller

Table 1. Values Obtained from the Diffusion Experiments

	t_{1d} (s)	t_{2d} (s)	$z \times 10^3$ (m)	$D \times 10^9$ (m^2/s)
Experiment 1				
Pattern 1	1980	7440	6.02	1.27
Pattern 2	1980	8940	6.13	1.23
Pattern 3	1980	12,240	6.60	1.27
Experiment 2				
Pattern 1	1726	3826	5.10	1.30
Pattern 2	1726	6826	6.02	1.43
Pattern 3	1726	11,626	6.34	1.30

The image capture times, turning point distances, and resulting diffusion coefficients are shown.

than the cell cross section, to ensure that the tablet could be placed in the cell cavity without jamming or breaking.

Results and Discussion

Calculation of the diffusion coefficient

A polynomial parameterization of the black lines in the interference patterns with respect to the pixels was fitted in MATLAB. The turning point distance was obtained by calculating and scaling the amount of pixels between the two points with zero derivatives. The diffusion coefficient for benzoic acid was then calculated from Eq. 8. The results are summarized below in Table 1. Figure 4 shows a typical interference pattern, where the turning point distance, z, is schematically shown.

The overall mean diffusion coefficient and standard deviation obtained from Table 1 are $\overline{D} = 1.30 \times 10^{-9}$ m^2/s and $\sigma_D = 6.87 \times 10^{-11}$ m^2/s, respectively, which is in agreement with previously published data.[27,28] It can thus be concluded that the values measured in the two experiments are consistent and that the different times at which the pictures were taken did not significantly affect the calculated diffusion coefficient. Using a $2\sigma_D$ variation, the results also indicate that the diffusion coefficient can be estimated with a minimum accuracy of about 10%. There are several simple methods available in the literature for measuring diffusion coefficients.[29] ESPI could be considered extensive or time consuming; however, there are important benefits as compared with other methods. Because some systems require stirring and diffusion to be measured indirectly via a porous frit, what is really measured is often nontrivial. The benefit of using ESPI is that the solution can be measured directly, leaving the system unperturbed during the whole experiment.

Estimation of the surface kinetics

Three dissolution experiments were conducted to calculate the surface kinetics. Two interference patterns from each experiment were then used to fit the surface kinetics to the tablet concentration profiles. Typical interference patterns at two different times are shown in Figures 5 and 6; the black vertical lines representing the discrete fringe positions to which the dissolution profile was fitted.

Because the amount of benzoic acid dissolved in each experiment was very small, the tablet interface was considered to be fixed. The interface can be seen as the left edge of the white region to the right in Figures 5 and 6. The fringes are packed more densely toward the interface, where the concentration gradient is relatively large and less densely further away into the black region where the concentration gradient is zero. The temperature was stable throughout the experiments, and there were no significant phase shifts in the interference patterns.[14] Therefore, from the interference

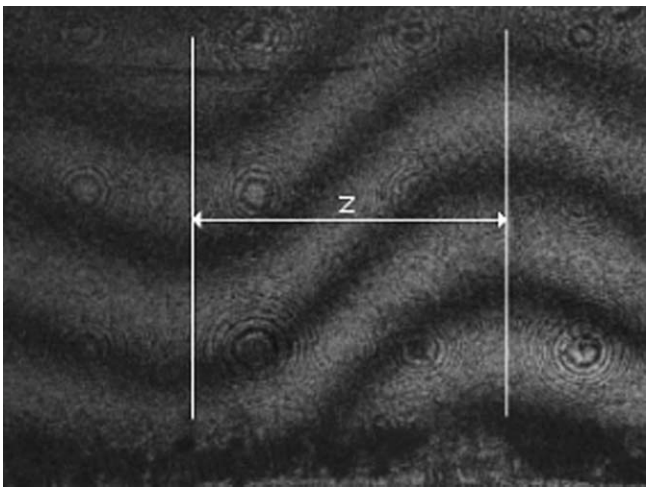

Figure 4. Typical interference pattern obtained from the diffusion experiments.

Vertical fringe introduction creates a turning point distance from which the diffusion coefficient can be calculated.

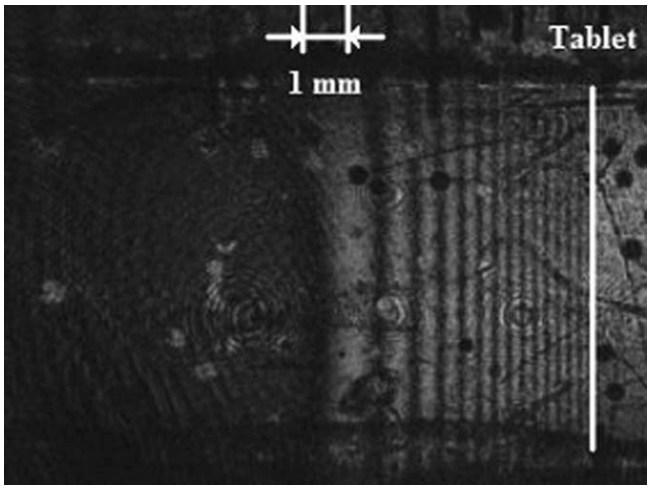

Figure 5. Typical interference pattern after ~1 h experimental time.

Fringes are closely packed toward the surface were the concentration gradient is relatively high. The image has been rotated 90° (see Figure 1).

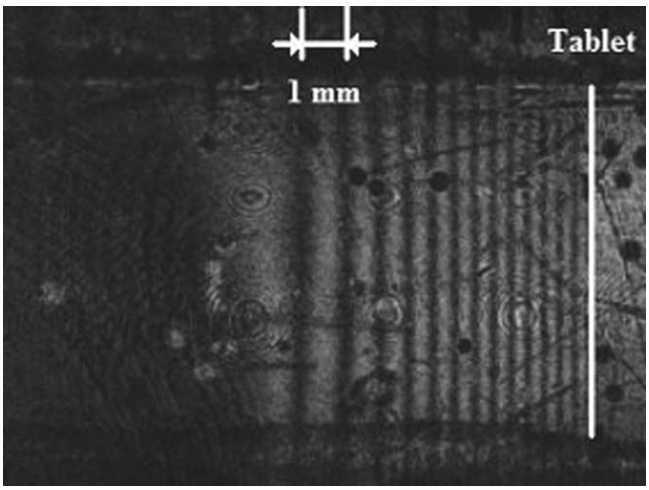

Figure 6. Typical interference pattern after ~2 h experimental time.

Diffusion has progressed and the fringe density is lower. The image has been rotated 90° (see Figure 1).

pattern, it was possible to directly calculate the concentration profile above the tablet. The black dots in both pictures are unfortunate yet insignificant air bubbles, formed on the external cell surfaces that could not be removed during the experiments.

Figures 7 and 8 show the experimental and fitted concentration profiles together with one of the experiments ~1 and 2 h after start. A $2\sigma_D$ variation from the estimated diffusion coefficient is also included. The fitted profiles were overall in good agreement with experimental data. However, the 1 h plot shows better agreement with experimental data than does the 2 h plot. This was also the case in the other two experiments.

Table 2 shows calculated values of the surface kinetics, including minimum and maximum values from the variation in diffusion coefficient. With the model assumptions, the maximum relative error from Table 2 implies an ideal accuracy of about 14% in the surface kinetics. This method can, therefore, serve as a tool in the characterization of tablet dissolution.

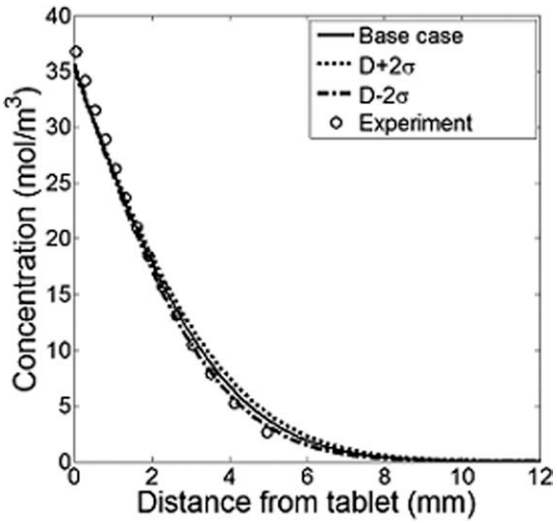

Figure 7. Fitted concentration profile according to model assumptions after ~1 h experimental time, including the variation of the diffusion coefficient.

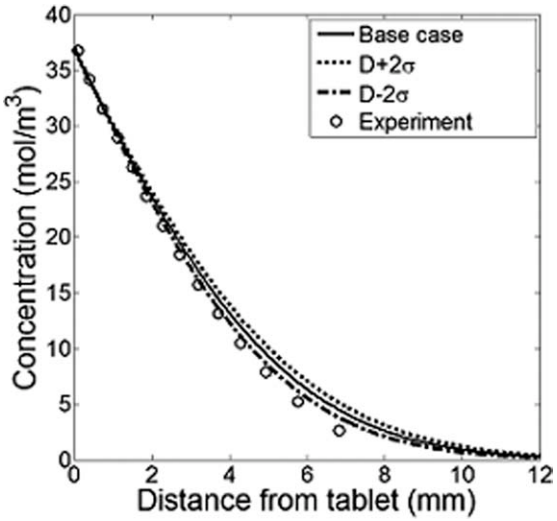

Figure 8. Fitted concentration profile according to model assumptions after ~2 h experimental time, including the variation of the diffusion coefficient.

The values from Table 2 can be directly compared with earlier work on dissolution of benzoic acid using a rotating disk, where the hydrodynamic mass-transfer coefficient constituted the dominating mass-transfer resistance, being up to one order of magnitude larger than the values obtained in this study.[24,30] For example, in Ref. 24, a value for the diffusion coefficient for benzoic acid at 30°C in 0.1 N HCl was determined to be $D = 1.6 \times 10^{-9}$ m^2/s, using the rotating disk method at 150 rpm, which is consistent with the value obtained in this study. However, the mass-transfer coefficient obtained in the same study was $k_m = 3.5 \times 10^{-5}$ m/s. The dissolution process is evidently mass transfer controlled in Ref. 24 and surface kinetics controlled in this study. The difference could be explained by the influence of hydrodynamic shearing (i.e., momentum transfer to the solid surface), adding erosion or affecting the properties at the solid–liquid interface when using a rotating disc apparatus. Thus, data obtained by using the rotating disk technique should be interpreted with care as the measured dissolution rate could include not only dissolution kinetics and external mass transfer but also strong influence from erosion due to hydrodynamic forces.

If the diffusion coefficient is also allowed as a fitting parameter, both early and later plots show better agreement. The values of the fitted surface kinetics, $k_s = 34.23 \times 10^{-7}$ m/s, and diffusion coefficient, $D = 1.01 \times 10^{-9}$ m^2/s, are significantly different as compared with the case with the fitted surface kinetics (Table 2) and measured diffusion coefficient

Table 2. Calculated Values for the Surface Kinetics, Including the Variation in the Diffusion Coefficient

	$k_s \times 10^{-7}$ (m/s)	$k_{s,min} \times 10^{-7}$ (m/s)	$k_{s,max} \times 10^{-7}$ (m/s)
Calculated value	23.8	21.7	27.1

(Table 1). Both parameters are also highly cross correlated, corr(D,k_s) = 0.69. The accuracy of the surface kinetics is, therefore, strongly dependent on the accuracy of the diffusion coefficient, making it necessary to measure the diffusion coefficient separately, as was made in this study. Because the diffusion coefficient has been accurately determined, the slight deviation between experimental and fitted data is negligible. Thus, the presented model is accurate enough to give insight into the diffusive as well as the kinetic process and furthermore shows that published data in the literature should be studied critically as the processes can be correlated.

Conclusions

The results from this study suggest that it is possible to characterize the kinetics of tablet dissolution using noninvasive ESPI technique. The distributed concentration profiles enable discrimination of the surface kinetics from the boundary layer mass transfer, thus avoiding lumping of dissolution parameters. The theoretical model showed good overall agreement with experimental data, resulting in plausible values for the surface kinetics. The current methodology can give further insight into the release mechanism and thereby contribute to the understanding of the release process. Furthermore, the influence of hydrodynamic shearing in dissolution tests can be explained and quantified.

A critical step in the suggested procedure is an accurate measurement of the diffusion coefficient, which in this study showed good agreement with existing published data. The low experimental variation in diffusion coefficient resulted in almost equal relative variation in surface kinetics, implicating a controllable error. It is also important to have accurate values for the solubility of the substance, because this will affect the concentration variation at the interface and thereby the calculated surface kinetics.

This methodology could be used to enhance the current understanding of the solid–liquid interface as well as dissolution parameters within the field of tablet dissolution. In a pharmaceutical context, the method could be used to characterize active substances and, under certain conditions, even to characterize multicomponent matrix or swelling transparent gel formulations. The two latter variants would require the use of multiple lasers at different wavelengths and a system having significant wavelength dependence in the refraction index.

Acknowledgment

The Swedish research council is gratefully acknowledged for their financial support.

Notation

Symbols

I = intensity distribution
U = electrical field
x = x coordinate (dimensionless)
y = y coordinate (dimensionless)
N = number of adjacent pixels
m = integer
n = refractive index
a = optical path, m
X = normal distance from tablet surface, m
b = cell thickness, m
i = fringe index
g = concentration/refraction index ratio, m^3/mol
c = concentration, mol/m^3
t = time, s
k = mass-transfer coefficient or surface kinetics, m/s
L = boundary, m
RSS = residual sum of squares, (mol/m^3)^2
D = diffusion coefficient, m^2/s
$\overline{D}$ = mean-diffusion coefficient, m^2/s
z = turning point distance, m
corr = correlation coefficient

Greek letters

ϕ = random phase difference, Rad
δ = change in phase difference, Rad
λ = wavelength, m
σ = standard deviation, m^2/s

Subscripts

1 = reference beam
2 = object beam
tot = total
i = fringe index
sat = saturation
mod = model value
exp = experimental value
low = low density solution
high = high density solution
1d = time for the first picture in the diffusion experiment
2d = time for the second picture in the diffusion experiment
D = diffusion coefficient
min = minimum value
max = maximum value
s = surface kinetics
m = mass-transfer coefficient

Literature Cited

1. Shiu GK. Dissolution methodology: apparatus and conditions. *Drug Inf J*. 1996;30:1045–1054.
2. Hixson AW, Crowell JH. Dependence of reaction velocity upon surface and agitation. I. Theoretical consideration. *Ind Eng Chem*. 1931;23:923–931.
3. Korsmeyer RW, Gurny R, Doelker E, Buri P, Peppas NA. Mechanisms of solute release from porous hydrophilic polymers. *Int J Pharm*. 1983;15:25–35.
4. Miranda JM, Pinheiro MNC, Campos JBLM. A simple model to obtain mass transfer coefficients from a soluble solid to a flowing fluid in closed recirculating systems. *Int Commun Heat Mass Transfer*. 2001;28:575–584.
5. Higuchi T. Rate of release of medicaments from ointment bases containing drugs in suspension. *J Pharm Sci*. 1961;50:874–875.
6. Colombani J, Bert J. Holographic interferometry for the study of liquids. *J Mol Liq*. 2007;134:8–14.
7. Bochner N, Pipman J. A simple method of determining diffusion constants by holographic interferometry. *J Phys D Appl Phys*. 1976; 9:1825–1830.
8. Szydloeska J, Janowska B. Holographic measurement of diffusion coefficients. *J Phys D Appl Phys*. 1982;15:1385–1393.
9. Karlsson D, Zacchi G, Axelsson A. Electronic speckle pattern interferometry—a tool for determining diffusion and partition coefficients for proteins in gels. *Biotechnol Prog*. 2002;18:1423–1430.
10. Axelsson A, Marucci M. The use of holographic interferometry and electron speckle pattern interferometry for diffusion measurement in biochemical and pharmaceutical engineering applications. *Opt Lasers Eng*. 2008;46:865–876.
11. Mattisson C. *Diffusion Studies in Gels Using Holographic Laser Interferometry, Chemical Engineering 1*. Lund, Sweden: Lund University, 1999.
12. Roger P, Mattisson C, Axelsson A, Zacchi G. Use of holographic laser interferometry to study the diffusion of polymers in gels. *Biotechnol Bioeng*. 2000;69:654–663.

13. Ruiz-Beviá F, Fernández-Sempere J, Colom-Valiente J. Diffusivity measurements in calcium alginate gel by holographic interferometry. *AIChE J*. 1989;35:1895–1898.
14. Marucci M, Pettersson S-G, Ragnarsson G, Axelsson A. Determination of a diffusion coefficient in a membrane by electronic speckle pattern interferometry: a new method and a temperature sensitivity study. *J Phys D Appl Phys*. 2007;40:2870–2880.
15. Marucci M, Ragnarsson G, Axelsson A. ESPI: a novel non-invasive tool for studying drug transport rate and drug permeability through free films. *J Controlled Release*. 2006;369–380.
16. Colombani J. Measurement of the pure dissolution rate constant of a mineral in water. *Geochim Cosmochim Acta*. 2008;72:5634–5640.
17. Doval AF. A systematic approach to TV-holography. *Meas Sci Technol*. 2000;11:R1–R36.
18. Gåsvik KJ. Computerized Optical Processes. In *Optical Metrology*, 3 ed. Chichester, U.K.: Wiley, 2002.
19. Zhang X, Hirota N, Narita T, Gong JP, Osada Y. Investigation of molecular diffusion in hydrogel by electronic speckle pattern interferometry. *J Phys Chem B*. 1999;103:6069–6074.
20. Mattison C, Karlsson D, Pettersson S, Zacchi G, Axelsson A. Light deflection and convection in diffusion experiments using holographic interferometry. *J Phys D Appl Phys*. 2001;34;3088–3096.
21. Apelblat A, Manzurola E, Bo Balal N. The solubilities of benzene polycarboxylic acids in water. *J Chem Thermodyn*. 2006;38:565–571.
22. Mooney KG, Mintun MA, Himmelstein KJ, Stella VJ. Dissolution kinetics of carboxylic acids. I. Effect of pH under unbuffered conditions. *J Pharm Sci*. 1981;70:13–22.
23. Compton RG, Harding MS, Pluck MR, Atherton JH, Brennan CM. Mechanism of solid/liquid interfacial reactions: the dissolution of benzoic acid in aqueous solution. *J Phys Chem*. 2002;97:10416–10420.
24. Grassi M, Grassi G, Lapasin R, Colombo I. *Understanding Drug Release and Absorption Mechanisms: A Physical and Mathematical Approach*. Boca Raton, FL: CRC Press, 2007.
25. The Mathworks, Inc. *MATLAB v. R2007b Documentation*. Natick, MA: The Mathworks, Inc., 2007.
26. Comsol AB. *Comsol Multiphysics User's Guide, v 3.5a*. Stockholm, Sweden: Comsol, 2008.
27. Delgado JMPQ. Molecular diffusion coefficients of organic compounds in water at different temperatures. *J Phase Equilib Diff*. 2007;28:427–432.
28. Lozar J, Laguerie C, Couderc JP. Diffusivité de l'Acide Benzoique dans l'Eau: influence de la temperature. *Can J Chem Eng*. 1975;53:200–203.
29. Cussler EL. *Diffusion: Mass Transfer in Fluid Systems*, 2nd ed. Cambridge: Cambridge University Press, 1997.
30. Kaunisto E, Nilsson B, Axelsson A. Drug dissolution rate measurements—evaluation of the rotating disc method. *Pharm Dev Technol*. 2009;14:400–408.

Manuscript received Aug. 16, 2010, and revision received Oct. 6, 2010.